Journal of Hydrology 534 (2016) 237–250

Contents lists available at ScienceDirect

Journal of Hydrology

journal homepage: www.elsevier.com/locate/jhydrol

Teleconnections of the ENSO and South Korean precipitation patterns

Jai Hong Lee *, Pierre Y. Julien

Department of Civil and Environmental Engineering, Colorado State University, Fort Collins, CO 80523, USA

ARTICLE INFO

Article history:
Received 27 October 2015
Accepted 7 January 2016
Available online 12 January 2016
This manuscript was handled by Andras Bardossy, Editor-in-Chief, with the assistance of Bruno Merz, Associate Editor

Keywords:
El Niño
La Niña
El Niño/Southern Oscillation
Precipitation

SUMMARY

The climatic relationship of the ENSO phenomena (El Niño/La Niña) and monthly precipitation patterns over South Korea is examined based on the composite and harmonic analysis. Three core regions, namely the Upper Region (UR), the Middle Region (MR), and the Lower Region (LR), were identified with a high level of the spatial coherence and temporal consistency rate, which represent the geographical extent and magnitude of the response of the ENSO forcing to the precipitation patterns. During the El Niño events, the February (+) to May (+), November (0) to April (+), and November (0) to May (+) wet period for UR, MR, and LR respectively, are the signal seasons having a high level of coherence and consistency. The spatial coherence rates of each region are 0.94, 0.98, and 0.98, and the temporal consistency rates are 0.80, 0.90, and 0.80 respectively. On the other hand, in case of the La Niña events, the October (0) to January (+), November (0) to May (+) dry period for UR and MR respectively, are the signal seasons showing a strong and consistent teleconnection. The spatial coherence rates of each region are 0.98, 0.96 and the temporal consistency rates are both 0.78. According to the comparative analyses for both extreme episodes, in three core regions, the El Niño/La Niña–precipitation relationships show the opposite sign, positive and negative precipitation anomalies respectively. Based on the results of annual cycle analysis, Mann–Whitney *U* hypothesis test and cross-correlation analysis, the wet anomalies during the warm event years, which prevail over the whole region, are more remarkable and significant than the dry departures during the cold event years. In conclusion, the climatic teleconnection between the extreme phase of SO and mid-latitude precipitation is identified over South Korea.

1. Introduction

El Niño and La Niña are opposite climate phenomena characterized by the unusual wide-ranging warming and cooling of the sea surface temperature ranging from the central to eastern tropical Pacific Ocean, due to the weakening and strengthening of the trade winds (easterlies) which blow predominantly through the eastern to the western Pacific by air pressure differences. These two types of fluctuations of the sea surface temperature are interactive with the Southern Oscillation (SO) defined as an atmospheric pressure circulation over the eastern–western equatorial Pacific with a periodic seesaw pattern. The interaction of the above oceanic fluctuation and atmospheric oscillation defines the El Niño/Southern Oscillation (ENSO), well known as a naturally occurring phenomenon involving fluctuating ocean temperatures over the central–eastern tropical Pacific Ocean, coupled with changes in the atmosphere (WMO, 2014).

Since the first approaches by Walker (1923) and Walker and Bliss (1932) to the impact of the extreme phase of SO on the variation of Indian monsoon rainfall, in the recent decades many global scale studies associated with ENSO showed remarkable climatic link between precipitation patterns and both warm and cold phases of Southern Oscillation (SO) in various areas of the world. Berlage (1966) showed the statistically significant correlations between climate indices of the SO and precipitation patterns in some regions of the globe, and Rasmusson and Carpenter (1983) revealed evidence of significant linkage between the evolution of the ENSO and anomalies in precipitation and surface temperature over the tropical Pacific. Moreover, more recent studies by Bradley et al. (1987), Ropelewski and Halpert (1987, 1989), and Kiladis and Diaz (1989), revealed noticeable ENSO–precipitation relationships with the identification of the seasons and regions having a consistent response of the warm and cold phases of SO to the precipitation pattern over the several regions of the globe. Also, Westra et al. (2013) investigated the presence of trends in annual maximum daily precipitation at global scale using Mann–Kendal test and generalized extreme value analysis for a significant association with globally averaged near-surface atmospheric temperature.

* Corresponding author. Tel.: +1 970 491 8824.
E-mail address: june.lee@colostate.edu (J.H. Lee).

http://dx.doi.org/10.1016/j.jhydrol.2016.01.011
0022-1694/

Much of the regional scale work relating the extreme phase of SO to hydrometeorological parameters over low and middle latitude by Douglas and Englehart (1981), Shukla and Paolino (1983), Rasmusson and Wallace (1983), Ropelewski and Halpert (1986), Redmond and Koch (1991), Kahya and Dracup (1994) and Price et al. (1998), found plausible evidence of strong and coherent links between ENSO and precipitation patterns. In detail, for mid-latitude regions, the importance of the ENSO–precipitation relationships is emphasized in several studies. Douglas and Englehart (1981), as well as, Ropelewski and Halpert (1986) reveal that ENSO is associated with enhancement of the winter precipitation in the southeastern United States, and the climatic relationship between low and high phases of SO and North American precipitation have been investigated by Ropelewski and Halpert (1986) and Kiladis and Diaz (1989). Dai (2013) examined the influence of the inter-decadal Pacific Oscillation (IPO) on United States precipitation using observational and reanalysis data and model simulations. Karabörk and Kahya (2003) detected coherent regions in Turkey where precipitation is associated with El Nino and La Nina events. Cai et al. (2011) diagnosed the impacts of ENSO on Australian rainfall from the perspective of tropical and extratropical teleconnections triggered by tropical SST variation and Power et al. (2006) examined the relationship between ENSO and all-Australian rainfall with a coupled general circulation model. Jin et al. (2005) identified statistically significant correlations between the extreme phases of SO and Korea–Japan precipitation patterns based on the cross-correlation analysis using the categorized SOI classified by five groups according to their magnitudes. Chandimala and Zubair (2007) investigated the predictability of seasonal rainfall for the Kelani river basin in Sri Lanka associated with ENSO and SST using correlation analysis and principal component analysis.

In South Korea, several recent studies exist concerning precipitation patterns associated with the ENSO events (El Niño/La Niña). Lee (1998) applied harmonic analysis to investigate the relationship between both extreme phases of SO and temperature/precipitation over South Korea. Cha et al. (1999) investigated the relationship between El Niño/La Niña events and the climate in Korea using synoptic data and ECMWF (European Centre for Medium-range Weather Forecasts) grid data, and showed that El Niño forcing has a tendency to modulate the precipitation over Korea by enhancing or suppressing with respect to seasons. Shin (2002) showed significant correlation between the warm/cold episodes and the floods/droughts in South Korea using statistically robust cross-correlation analysis.

As seen from the above, the majority of previous global/regional scale studies have focused on mostly the Pacific Rim countries. These studies revealed the significant teleconnection between the ENSO forcing and hydrometeorological variations in the lower to mid latitudes. However, the impact of El Nino and La Nina events on the mid to high latitudes is not clear. The global scale study by Ropelewski and Halpert (1987, 1989) showed significant ENSO–precipitation relationship in some regions over the globe, with some potential for the signal over the East Asia. According to a visual inspection of station locations in the above study, the existence of the ENSO signals is not clearly identified in South Korea due to the limitation of data coverage. This indicates the need for a diagnostic investigation, supported by adequate and sufficient dataset, of the impact of ENSO forcing over South Korea.

The main objectives of this investigation are to: (1) identify coherent, consistent, and significant response of the warm extreme phase of SO (El Niño) to the precipitation patterns over South Korea, using a composite and harmonic analysis based on the improved description of the magnitude, phase, and geographical extent of the ENSO-related precipitation response; (2) investigate the climatic link between the precipitation patterns and the cold extreme phase of SO (La Niña) using the same composite and harmonic analysis as the above El Niño case; (3) examine the comparison between El Niño and La Niña–precipitation relationships with the viewpoint of intensity and trend of the significant responses, by comparative analyses such as an annual cycle analysis, a Mann–Whitney *U* hypothesis test, and a cross-correlation analysis.

2. Data set and methodology

2.1. Data set

The time series of monthly precipitation records applied in this analysis *are* based on 76 stations distributed all over South Korea. The source of these dataset is Korea Meteorological Administration (KMA) which is a governmental organization under the Ministry of Environment (MOE) monitoring and operating the overall Korean meteorology. The time series extend from 1904 to 2014 and cover more than about 20 episodes of El Niño and La Niña. Not only the meteorological stations with missing data for more than a season were excluded, but also the stations with less than 42 years of data or spanning less than 9 ENSO events were ruled out from the analysis. Finally, by taking the temporal persistency and spatial distribution into consideration, a subset of 60 gauging stations are selected in this study (Fig. 1).

In order to detect a consistent influence of ENSO episodes on precipitation pattern over South Korea, a wide set of ENSO events is selected by a comprehensive range of criteria based on the definition and classification by Quinn et al. (1978), Rasmusson and Carpenter (1983), Ropelewski and Halpert (1987, 1989), Kiladis and Diaz (1989), and Trenberth (1997). The overall ENSO years applied in this analysis are displayed in Table 1.

As a method of representing large-scale climate fluctuation over the Pacific Ocean, a climatic index known as the Southern Oscillation Index (SOI) is employed. The time series of SOI are calculated using the difference of the standardized anomalies of the sea level atmospheric pressures between the Tahiti and Darwin, Australia. The time series of SOI calculated by the NOAA Climate Prediction Center is applied in the present study.

2.2. Methodology

The methodological approach for understanding and predicting teleconnection patterns consists of empirical orthogonal teleconnection (EOT), cross correlation analysis, mean *t*-test and harmonic analysis (e.g., Klingaman et al., 2013; King et al., 2014; McBride and Nicholls, 1983; Jin et al., 2005; Kahya and Dracup, 1994; Ropelewski and Halpert, 1986, 1987). In this present study, to provide a logical extension of the global scale study associated with the ENSO–precipitation teleconnection, an empirical methodological approach designed by Ropelewski and Halpert (1986, 1987) is applied with some changes and additions.

Fig. 2 shows the schematic description for the overall methodology used in this study, based on Ropelewski and Halpert (1986, 1987). The detailed procedures of the methodology comprise primarily three stages, namely, data processing, analytical method application, and comparative analysis stage. The first stage is intended for transforming the original raw data into an appropriate data format such as SPI, non-exceedance probability series, categorized SOI, and modular coefficients. The second stage is to detect candidate regions and confirm core regions based on composite and harmonic analysis. And the last stage is focused on the comparative interpretation on El Niño and La Niña–precipitation relationships using annual cycle analysis, Mann–Whitney *U* test, and cross-correlation analysis.

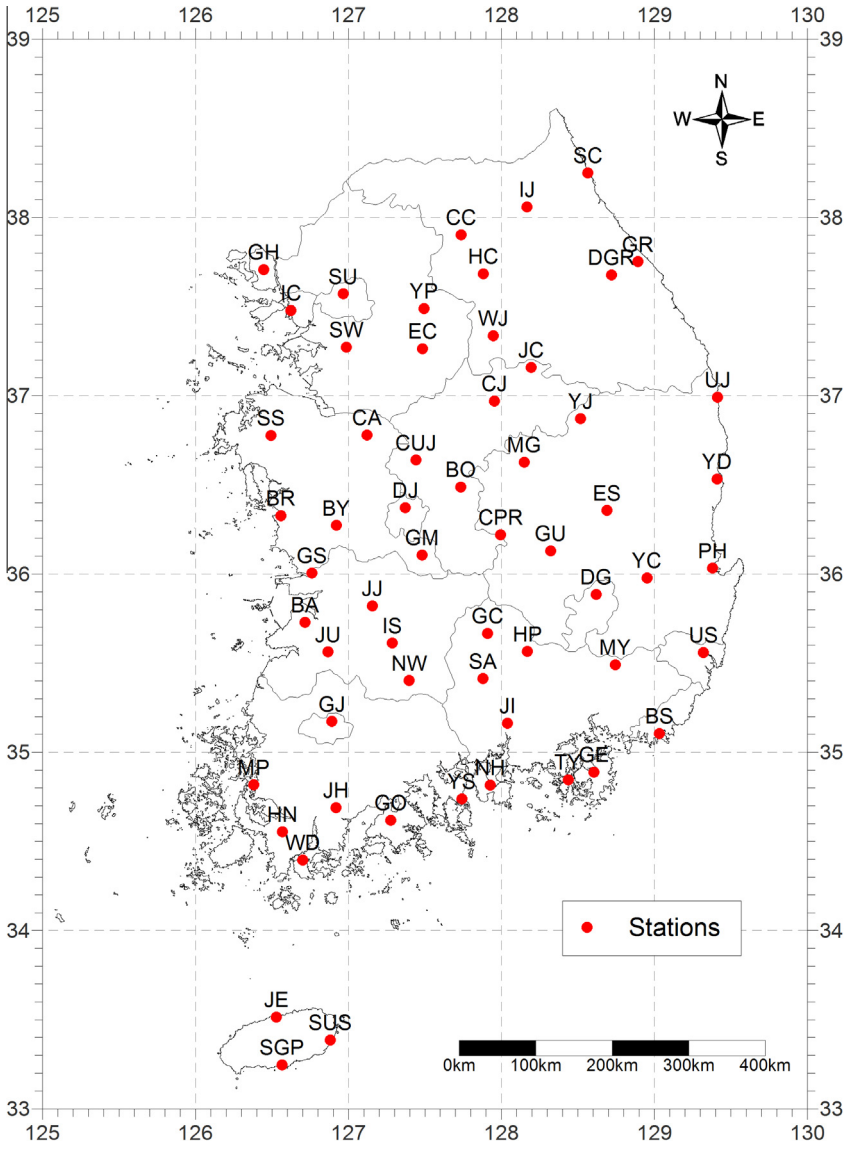

Fig. 1. Stations used for precipitation indices.

Table 1
List of the ENSO episode years included in this study.

El Niño years	La Niña years
1905, 1911, 1914, 1918, 1923, 1925, 1930, 1932, 1939, 1941, 1951, 1953, 1957, 1963, 1965, 1969, 1972, 1976, 1982, 1986, 1991, 1994, 1997, 2002, 2004, 2006, 2009	1910, 1915, 1917, 1924, 1928, 1938, 1950, 1955, 1964, 1971, 1973, 1975, 1985, 1988, 1995, 1998, 2000, 2005, 2007, 2010

2.2.1. Data processing

For the composite and harmonic analysis to identify the ENSO response to the local precipitation patterns, the original monthly precipitation data were transformed into Standardized Precipitation Index (SPI), which is widely known as a drought index developed to assess the drought phenomena effectively. The SPI estimated by McKee et al. (1993), which is recommended by World Meteorological Organization (WMO, 2012), is a probability index based on a statistical fit to an appropriate probability density function and a transformation into standardized normal distribution. The SPI is not only fairly easy to compute since the only input data is precipitation, but also simple to compare in terms of space and time due to being provided as dimensionless index values. In addition, another advantage of the SPI is that it is spatially consistent and analytical for probabilistic process (Guttman, 1998).

In this study, the monthly precipitation data of 60 meteorological stations over South Korea are fitted to a gamma distribution for calculating the SPI following the approach of McKee et al. (1993). The associated cumulative density function (CDF) is estimated from the fitted distribution and subsequently transformed into a CDF of the standard normal distribution by the equal-probability transformation. The SPI time series, which can be used in the composite and harmonic analysis, are calculated using the resulting standard deviates of the transformed CDF with a mean of zero and standard deviation of unity.

In order to examine the quantitative and significant impact of the Southern Oscillation Index (SOI) on precipitation patterns over South Korea, the cross-correlation coefficients are calculated between the categorized SOI and the seasonal precipitation series. In this analysis, four seasonal averages of SOI and precipitation data are formed according to three months averaged seasons, which is defined as: boreal winter (December–February), spring

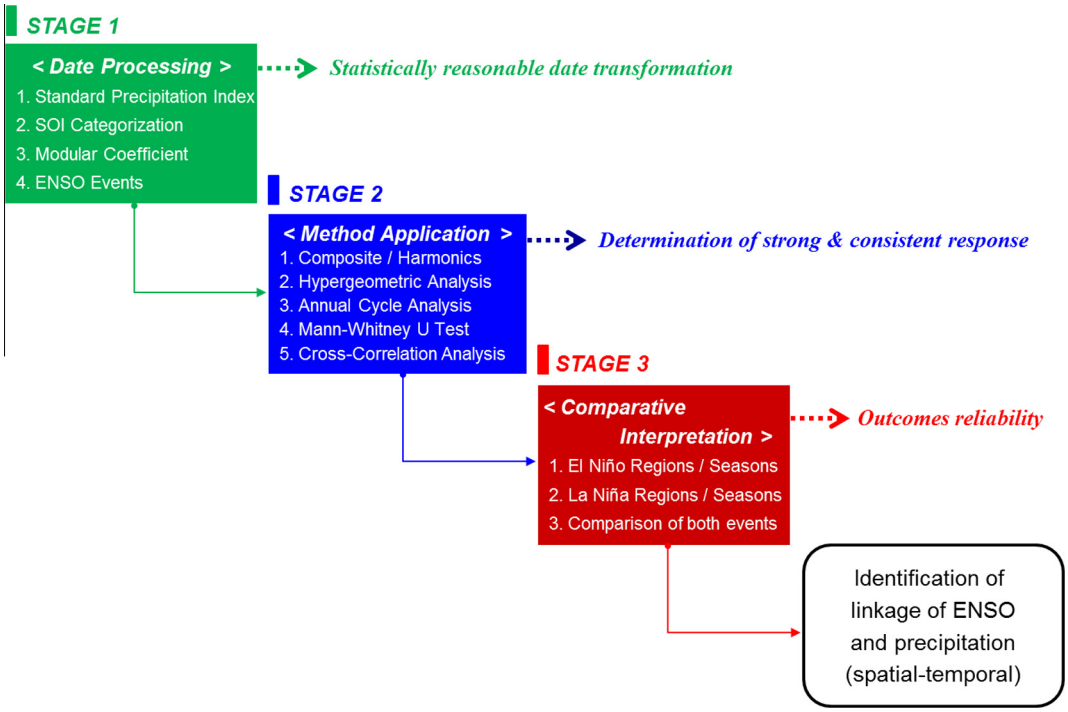

Fig. 2. Flowchart presentation of the empirical methodology consisting of three stages.

(March–May), summer (June–August), and fall (September–November). Prior to the correlation analysis, the data for each individual season are converted into non-exceedance probability time series to deal with the disparities among stations and to get rid of periodicities in the time series. The non-exceedance probability can be obtained using the Weibull plotting position formula. The entire precipitation data for each individual season are ranked from the smallest amount to the largest amount, and then divided by $n+1$ (n is the number of data). Subsequently, the resulting associated values are the non-exceedance probability time series for each season. In addition, the SOI is classified into five categories based on the magnitudes of each data following the suggestion of Jin et al. (2005). The SOI values are assigned to each category which is grouped into five levels in accordance with the magnitude: Strong La Niña (SOI > 2), Weak La Niña ($1 < \text{SOI} \leqslant 2$), Normal Phase ($-1 \leqslant \text{SOI} \leqslant 1$), Weak El Niño ($-2 \leqslant \text{SOI} < -1$), and Strong El Niño (SOI < −2).

For annual cycle analysis, the monthly precipitation data are converted to modular coefficients to remove the effect of dispersed mean and variance values, through the use of expressing monthly precipitation values as percentages of mean annual values. The time series of modular coefficient are obtained by the proportion of the original precipitation data to the monthly mean data, which are averaged over the total data series, to place all stations on a same basis with invariable condition of the cyclic feature of the values, simultaneously.

2.2.2. Method application

For composite analysis, as a approach to describe the general patterns of the ENSO-related precipitation behavior, the 24-month ENSO composites are formed for each station, starting from the July of previous year of the events designated as July (−), through the event years designated as (0), to the June of subsequent year of the events designated as June (+), based on Ropelewski and Halpert (1986, 1987). By means of averaging the converted precipitation data for the all proposed ENSO episodes on an equal basis, the final ENSO composite is calculated.

The time series of 24-month ENSO composite are subjected to a harmonic analysis representing a periodic function by the summation and integration of a series of trigonometric functions. Harmonic analysis applied first in investigating the climatic precipitation regimes by Horn and Bryson (1960) has been considered as an objective and analytic approach to examining precipitation seasonality. Fig. 3 shows an example of four harmonics for annual variation based on Scott and Shulman (1979), and the sample harmonic fits for the same period using the SPI previously converted from original precipitation data. According to the assumption that the only one maximum or minimum value of precipitation data is corresponded to the extreme ENSO forcing, the first harmonic is extracted from the 24-month ENSO composite with the amplitude and phase of the ENSO-related precipitation signal. In this first harmonic curve, the amplitude indicates the representative magnitude of the precipitation response to ENSO events, and the phase angle refers to the time showing a maximum departure from the mean value in the first harmonic cycle (Fig. 4). The first harmonic is fitted as follows based on Wilks (1995):

$$X_t = \overline{X} + \sum_{k=1}^{N/2}\left\{C_k \cos\left[\frac{2\pi kt}{N} - \varnothing_k\right]\right\} = \overline{X} + \sum_{k=1}^{N/2}\left\{A_k \cos\left[\frac{2\pi kt}{N}\right] + B_k \sin\left[\frac{2\pi kt}{N}\right]\right\} \quad (1)$$

where

$$A_k = \frac{2}{N}\sum_{t=1}^{N} X_t \cos\left(\frac{2\pi kt}{N}\right) \quad (2)$$

$$B_k = \frac{2}{N}\sum_{t=1}^{N} X_t \sin\left(\frac{2\pi kt}{N}\right) \quad (3)$$

where X_t is the SPI value at time t, t is the time of observation, $\overline{X}$ is the mean value of the SPI, k is the harmonic number (the first harmonic, $k = 1$), N is the sample size (period), C_k is the maximum deviation from the mean value, $\varnothing_k$ is the time when the harmonic

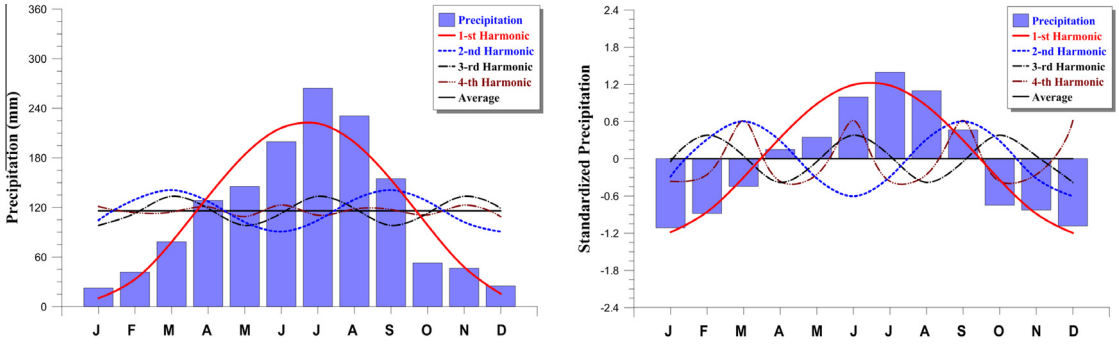

Fig. 3. An example illustrating the interpretation of the annual cycle at a station with pronounced wet season. Left figure is the harmonic fit of monthly precipitation and right one is the harmonic fit of standardized precipitation index of station no. 279 applied in this study.

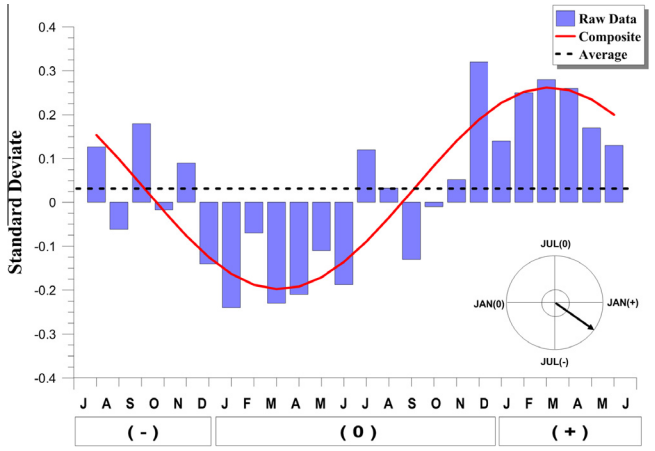

Fig. 4. A first harmonic fit to the precipitation El Niño composite for the gauging station no. 279 in South Korea. The amplitude and the phase of the first harmonic are presented as a harmonic dial. The dial refers to the amplitude of 0.25 and the phase of March (+).

has a maximum, and A_k and B_k are the Fourier coefficients. The term C_k and $\varnothing_k$ represent the amplitude and the phase shift of the harmonic, given by

$$C_k = \left(A_k^2 + B_k^2\right)^{0.5} \tag{4}$$

And

$$\varnothing_k = \begin{cases} tan^{-1}\frac{B_k}{A_k}, & A_k > 0 \\ tan^{-1}\frac{B_k}{A_k} \pm \pi, \text{ or } \pm 180^\circ, & A_k < 0 \\ \frac{\pi}{2}, \text{ or } 90^\circ, & A_k = 0 \end{cases} \tag{5}$$

The information included in harmonic curves can be effectively summarized as a graphical device known as the harmonic dial, which is useful for representing the geographic trends of periodic parameters. The first harmonic is expressed as a vector having the length and direction (angular orientation), which represent the intensity and timing of the maximum response of the ENSO forcing to the precipitation patterns, respectively, and then is represented as a harmonic dial (Hsu and Wallace, 1976). According to the map of harmonic dials, the "candidate regions" showing spatially coherent ENSO-related precipitation signal are identified.

The harmonic dials are useful to identify the candidate regions by detecting a group of vectors having the similar strength and direction, but are not sufficient to clearly identify the consistency of the ENSO–precipitation relationship. The spatial coherence is employed to determine the candidate regions having coherent harmonic vectors, and is estimated through the following calculation based on Ropelewski and Halpert (1986, 1987) and Kahya and Dracup (1993):

$$C = \frac{[V]}{S} \tag{6}$$

$$[V] = \frac{\left[\left(\sum V\cos\theta\right)^2 + \left(\sum V\sin\theta\right)^2\right]^{1/2}}{L}, \quad S = \frac{\sum V}{L} \tag{7}$$

where $[V]$ is the average vector of the individual components of the harmonic vectors in the proposed candidate regions, S is the average of the individual vector magnitudes, V is the magnitude of the vector, θ is the angular orientation of the vector, and L is the total number of vectors within the regions. The coherence of zero indicates that a group of vectors show the same magnitude in different directions, while the value of one refers to that all vectors have the same direction, but do not necessarily all have the same magnitude (Brooks and Carruthers, 1953). Candidate regions were identified based on the coherence of the order of 0.85 or greater to eliminate the inconsistency between amplitudes and phases of the vectors following the approach of Halpert and Ropelewski (1992).

In order to examine the ENSO-related signal season showing the consistent and apparent response of the ENSO forcing to the precipitation patterns, the aggregate composites are formed by spatially averaging the entire ENSO composites within each candidate region. The aggregate composites are plotted based on a 36-month period following the approach of Kahya and Dracup (1993), to detect more accurately the signal season and to cover the entire life cycle of the ENSO events.

According to the aggregate composite, only one season within the ENSO cycle based on the aforementioned assumption that the first harmonic has one maximum and minimum value during the ENSO cycle, is detected by means of searching a group of anomalies having the same sign for more than four consecutive months at least. Taking the distance between the tropical Pacific Ocean and the study area located in the mid-latitude into consideration, it is reasonable to regard the responding period of ENSO forcing as the event year and the subsequent year of the event.

In order to examine the consistency of the ENSO-related precipitation signal and calculate the correlation between the ENSO forcing and precipitation patterns, another time series of the monthly precipitation values, is employed based on the candidate regions and detected seasons previously obtained from the aggregate composites. These index time series (ITS) are formed not only by regional average of the precipitation data over the all stations, but also by temporal average for all years of record.

Finally, for the purpose of determining a core regions, which is defined as a region having a strong and consistent precipitation responses to the ENSO episodes, within the candidate regions previously detected from the harmonic dial, the rate of temporal consistency is calculated based on the proportion of number of years in the ITS having the ENSO-related precipitation signal to the number of total ENSO years.

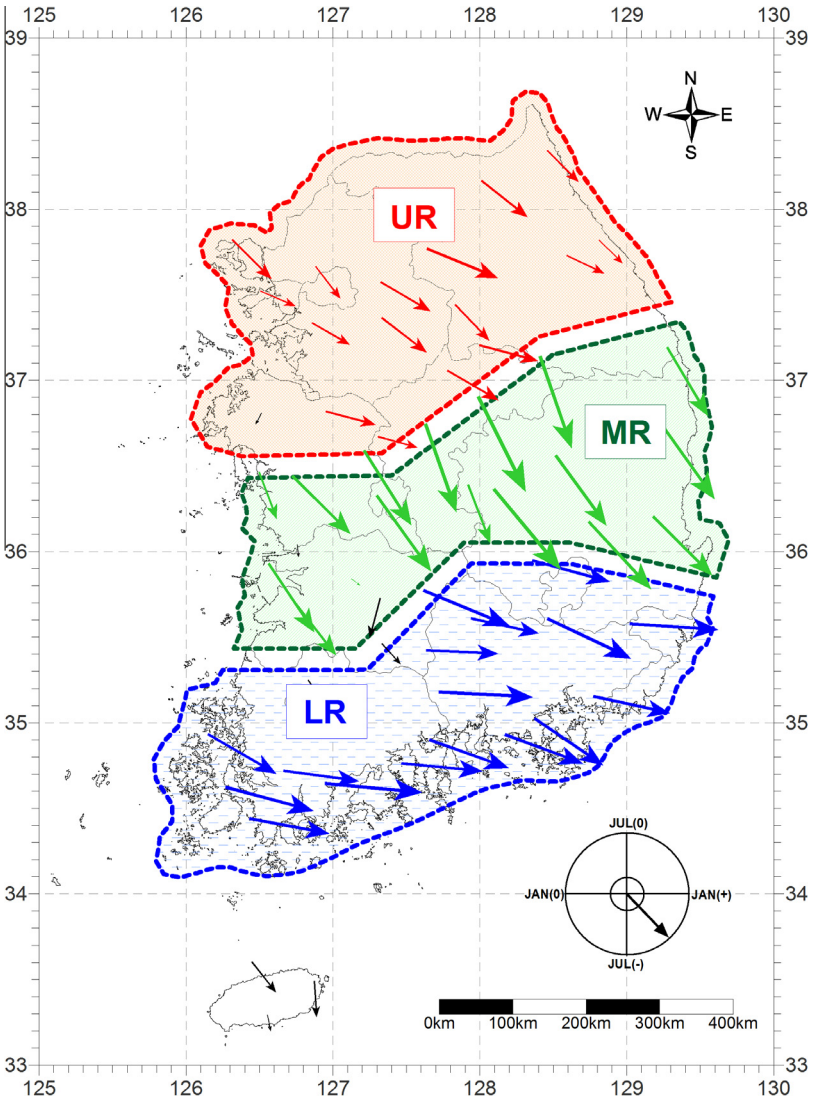

Fig. 5. Precipitation vectors based on the 24-month harmonic fitted to El Niño composites. Scale for the direction of arrows: south, July (−); west, January (0); north, July (0); and east, January (+). The magnitude of arrows is proportional with the amplitude of the harmonics.

Table 2
Properties of the candidate regions (El Niño events).

Region	Season	Coherence	Total episode	Occurrence episode	Consistency (%)	Extreme events
UR	February (+)–May (+)	0.94	10	8	80	3
MR	November (0)–April (+)	0.98	10	9	90	4
LR	November (0)–May (+)	0.98	10	9	80	4

Ropelewski and Halpert (1986) examined the occurrence of extreme precipitation events with relation to the ENSO–related precipitation response to check the climatic link between the ENSO phenomena and the extreme phase of precipitation. Following this context, in this study the number of extreme precipitation occurrences in association with ENSO episodes during the signal season is counted. In order to assign the limits of the level, the ITS values are ranked from the largest amount to the smallest amount, normalized by the amount of the total data, and then converted to the probability from the Weibull plotting position formula. The highest level is designated with the probability of ITS equal to 80%, while the lowest level with the probability of ITS equal to 20% (Kahya and Dracup, 1994).

2.2.3. Comparative analysis and interpretation

As an effective method of assigning the significance level of the ENSO–precipitation relationship, the hypergeometric distribution test is employed, which is a statistical approach calculating the probability of a random occurrence of the signal season during the ENSO event. Haan (1977) calculated "the cumulative probability that at least m successes are obtained in n trials from a finite population of size N containing k successes" using the hypergeometric distribution test. In this study, the test is carried out in two cases (A and B) according to the definition of a success. For the ENSO–precipitation relationship, a success means the occurrence of an ITS value above (below) the median in case A, while a success means that of a wettest (driest) ITS value larger (smaller) than 80% (20%)

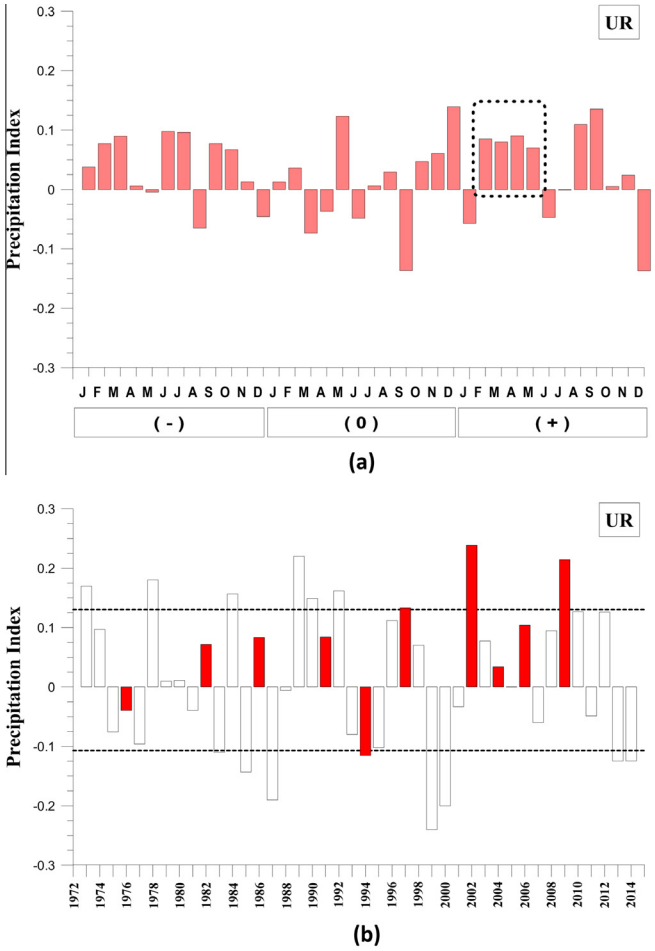

Fig. 6. (a) El Niño aggregate composite for the candidate UR region. The dashed line box delineates the season of possible El Niño-related responses. (b) The index time series for the UR region for the season previously detected. El Niño years are shown by solid bars. The dashed horizontal lines are the upper (80%) and lower (20%) limits for the distribution of ITS values.

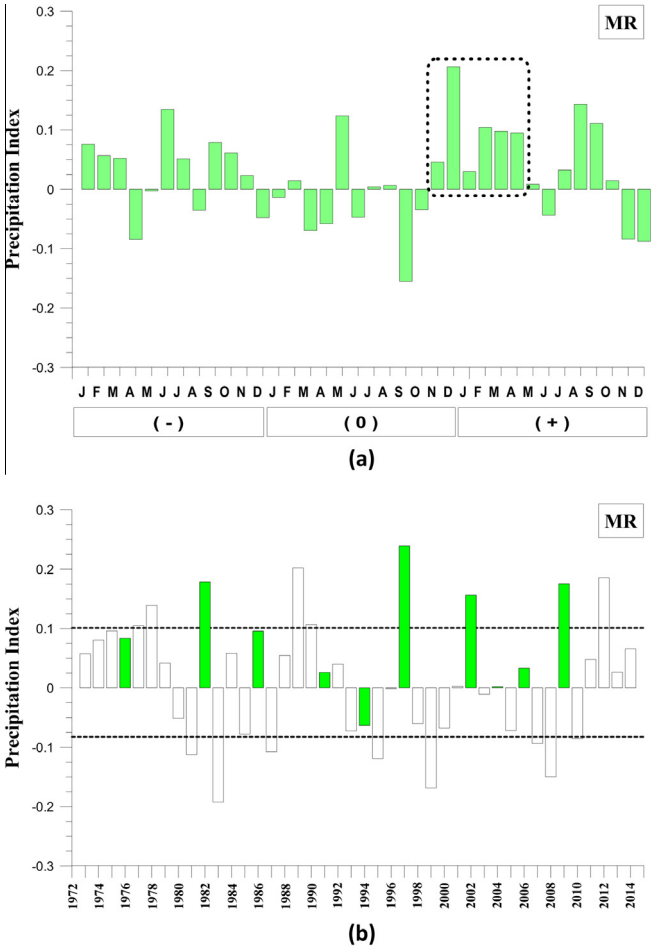

Fig. 7. As in Fig. 6, except for the candidate MR region.

value in case B, following the suggestion of Kahya and Dracup (1994).

The annual cycle analysis on the basis of the approach of Kahya and Dracup (1993) is applied to this study to compare the signal seasons of the warm and cold episodes in terms of the intensity and trend of the response. In this analysis, the monthly precipitation data are converted to modular coefficients, which are obtained by the proportion of the original precipitation data to the monthly mean data, which are averaged over the total data series. These resulting data sets place all stations on a same basis with invariable condition of the cyclic feature of the values, and are checked whether the El Niño/La Niña forcings modulate the precipitation patterns by increasing or decreasing.

For the purpose of checking a significant difference in the magnitude of both extreme phase-related precipitation signals, a statistical hypothesis test using the Mann–Whitney *U* approach is carried out. The two datasets are collected regarding the extreme phases of ENSO (El Niño and La Niña episodes), and then the null hypothesis is assumed as the equality of the two datasets. According to the result of the rank-sum hypothesis test, the quantitative and noticeable difference between the two datasets can be identified.

As another comparative method for the El Niño/La Niña–related precipitation signals, the cross-correlation analysis is employed on the basis of seasonal comparison between the large-scale climate index (categorized SOI) and the monthly precipitation data (non-exceedance probability). These resulting cross-correlation coefficients are used to examine the intensity and the trend (positive or negative) of the ENSO–Precipitation correlation. A more detailed explanation of the analysis was given in the first stage of data processing.

3. Results and discussion

3.1. El Niño–precipitation relationship

Fig. 5 shows the results of detecting the candidate regions based on a harmonic dial map resulting from the composite and harmonic analysis. According to the harmonic dial map, the overall study area is grouped into three candidate regions, namely from north to south: the Upper Region (UR), the Middle Region (MR), and the Lower Region (LR). For these candidate regions, the overall results of determining the core region using the rate of temporal consistency are outlined in Table 2. The first column of data indicates the candidate regions and the second column is the signal season. The third column of data shows the results of spatial coherence, the fourth to sixth column present the results of the temporal consistency, and the last column of data shows the number of extreme precipitation occurrences associated with the ENSO events.

3.1.1. Upper Region (UR)

The UR region has a spatial coherence of 0.94. In Fig. 6(a), the aggregate ENSO composite of the UR region indicates a tendency for above normal precipitation, i.e., larger than the 50% value, during the February (+) to May (+). The period outlined by the dashed lines represents the season having a significant ENSO–related

precipitation signal. The index time series (ITS) for the previously identified season show that eight out of ten El Niño episodes are associated with wet conditions at a consistency rate of 0.80 as described in Fig. 6(b). Based on the highest limit (80%) and lowest limit (20%) for the ITS values, which is drawn by the dashed lines in Fig. 6(b), three of nine extremely wet precipitation occurrences are associated with the El Niño episodes. It is evident from the results presented here that the UR region is evaluated as a core region with a coherent and consistent El Niño–precipitation relationship.

3.1.2. Middle Region (MR)

The coherence value of the MR region is 0.98. The aggregate ENSO composite of the MR region shows that wetter conditions are related to the El Niño phenomena for the November (0) through April (+) as shown in Fig. 7(a), in which the period outlined by the dashed lines indicates the season having ENSO–precipitation response. The ITS for the signal season reveals that nine out of ten warm episodes represent the wet season indicating a high rate of consistency (0.90) as shown in Fig. 7(b). Four out of nine occurrences of wettest years with values of equal to or larger (smaller) than 80% (20%) value, are associated with the El Niño episodes, using the highest and lowest limits for the ITS values, which is drawn by the dashed lines in Fig. 7(b). It is clear from these results that the MR region is considered as a core region with a strong and consistent relationship between the warm episode of ENSO and precipitation pattern.

3.1.3. Lower Region (LR)

The spatial coherence of the LR region is equal to 0.98. According to Fig. 8(a), the aggregate ENSO composite of the LR region shows that wet conditions occur during the November (0) to May (+) season. The period drawn by the dashed lines indicates the season of possible ENSO–precipitation relationship. The ITS for the previously detected season shows that nine out of ten El Niño episodes are associated with wet conditions with a high level of consistency (0.90) as described in Fig. 8(b). Based on the highest limit and lowest limit, 80% and 20% for the ITS values which is drawn by the dashed lines in Fig. 8(b), four of nine extremely wet precipitation occurrences are associated with the El Niño events. It is therefore plausible to suggest that the LR region is accepted as a core region with a strong and consistent El Niño–pre cipitation relationship.

3.2. La Niña–precipitation relationship

As a result of searching the candidate regions, a harmonic dial map based on the composite and harmonic analysis is described in Fig. 9. In the harmonic dial map, three candidate regions, namely from north to south: the Upper Region (UR), the Middle Region (MR), and the Lower Region (LR) are detected. For these candidate regions, the overall results of determining the core region using the rate of temporal consistency are outlined in Table 3. The first to last columns present the same as those in Table 2.

3.2.1. Upper Region (UR)

The spatial coherence of the UR region is equal to 0.98. In Fig. 10 (a), the aggregate ENSO composite of the UR region indicates a tendency for below normal precipitation, i.e., smaller than the 50% value, during the October (0) to January (+). The range outlined by the dashed lines represents the season having a significant ENSO–related precipitation signal. The index time series (ITS) for the previously identified season show that seven out of nine La Niña episodes are associated with dry conditions at a consistency rate of 0.78 as described in Fig. 10(b). Based on the highest limit (80%) and lowest limit (20%) for the ITS values, which is drawn by the dashed lines in Fig. 10(b), five of eight extremely dry

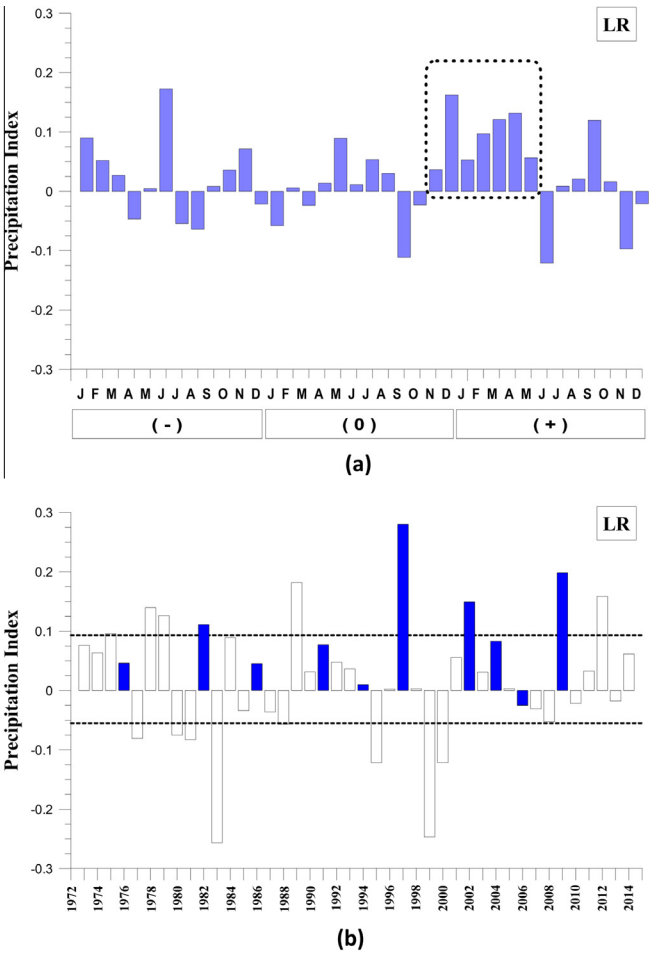

Fig. 8. As in Fig. 6, except for the candidate LR region.

precipitation occurrences are associated with the cold phase of SO. It is evident from the results presented here that the UR region is evaluated as a core region with a coherent and consistent La N iña–precipitation relationship.

3.2.2. Middle Region (MR)

The coherence value of the MR region is 0.96. The aggregate ENSO composite of the MR region shows that drier conditions are related to the La Niña phenomena for the November (0) through May (+) as shown in Fig. 11(a), in which the period outlined by the dashed lines indicates the season having ENSO–precipitation response. The ITS for the signal season reveals that seven out of nine La Niña events represent the wet season indicating a reasonable rate of consistency (0.78) as shown in Fig. 11(b). Three out of eight occurrences of driest years with values of equal to or larger (smaller) than 80% (20%) value, are associated with the La Niña episodes, using the upper and lower limits for the ITS distribution values which is drawn by the dashed lines in Fig. 11(b). It is therefore plausible to suggest that the MR region is considered as a core region with a strong and consistent relationship between the La Niña and precipitation patterns.

3.2.3. Lower Region (LR)

Although the coherence of the LR region is equal to 0.94, the season of potential ENSO–precipitation relationship was not detected based on the aggregate composite and the ITS distribution. Consequently, the LR region is found to be not accepted as a core region associated with the cold events.

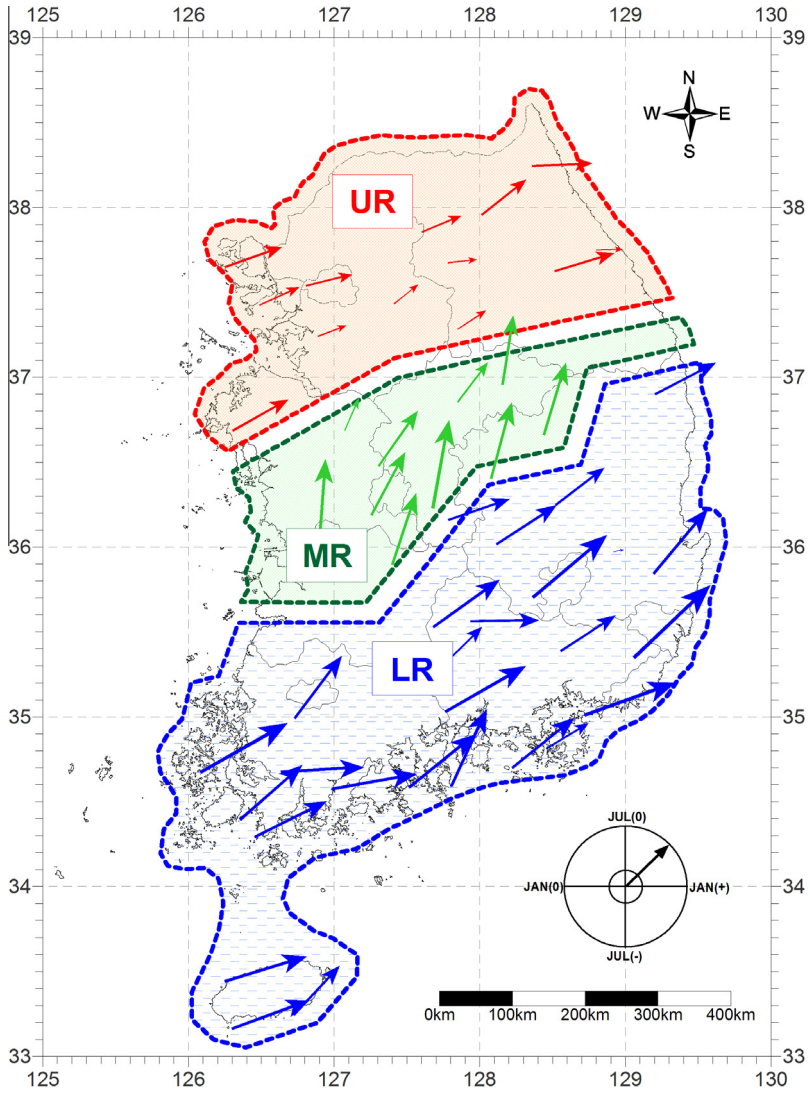

Fig. 9. As in Fig. 5, except for La Niña composites.

Table 3
Properties of the candidate regions (La Niña events).

Region	Season	Coherence	Total episode	Occurrence episode	Consistency (%)	Extreme events
UR	October (0)–January (+)	0.98	9	7	78	5
MR	November (0)–May (+)	0.96	9	7	78	3

3.3. Comparative analysis of El Niño and La Niña

Table 4 shows the results of calculating the probability of a random occurrence of the signal season during the warm episodes based on the hypergeometric distribution test. In case A, all regions indicate a statistically significant relationship with a high significance level (between 94% and 98%), based on a very low chance of random occurrence of the ITS value above the median for the El Niño events. Additionally, in case B, based on a very low chance of random occurrence of the wettest ITS value larger than 80% value for the El Niño events, the relationship of all regions result in a high significance level of 93%, except for the UR region (79%). On the other hand, the results of calculating the probability during the cold events by the hypergeometric distribution model are outlined in Table 5. The relationships of both regions for case A are found to be highly significant at the 96% and 98%, considering very low chance of random occurrence of the ITS value below the median for the La Niña events. In case B, the UR regions shows a highly significant relationship with a 100% significance level, based on a very low chance of random occurrence of the driest ITS value smaller than 20% value for the La Niña events, while the significance level of the MR region is calculated as 87%. Thus, the analyses for the two extreme events show similar results indicating a high statistical significance level for the above/below normal precipitation.

Fig. 12 illustrates the relationship between the El Niño composite cycle and the annual precipitation cycle plotted by modular coefficients. Since a consecutive above normal precipitation period for the El Nino signal season is detected in the El Niño–annual precipitation cycle, it is plausible that the El Nino forcing modulates precipitation by enhancing its magnitude in the UR, MR, and LR region, respectively. Based on the conversion of precipitation date

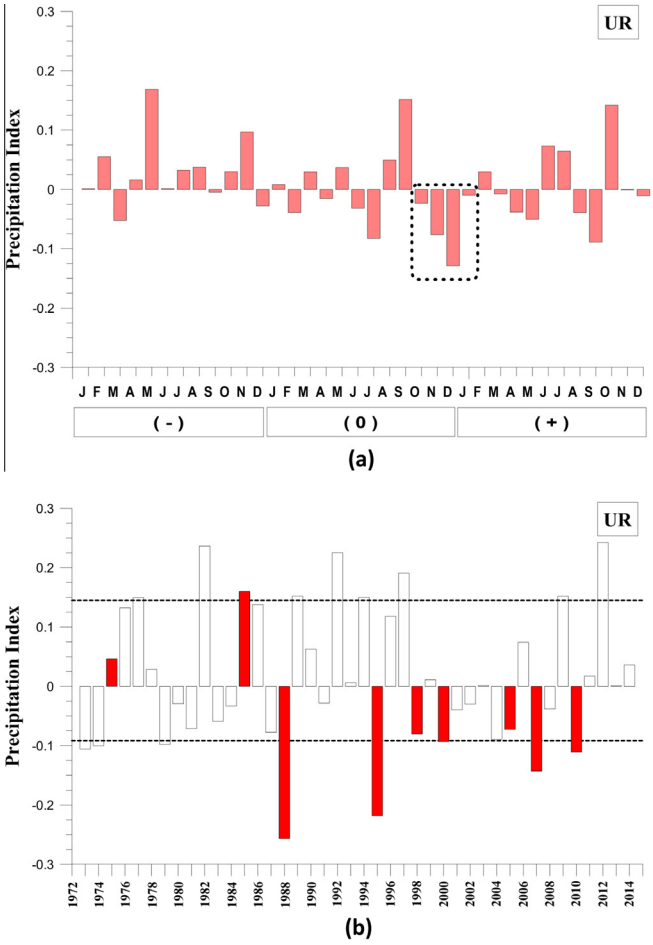

Fig. 10. (a) La Niña aggregate composite for the candidate UR region. The dashed line box delineates the season of possible La Niña-related responses. (b) The index time series for the UR region for the season previously detected. La Niña years are shown by solid bars. The dashed horizontal lines are the upper (80%) and lower (20%) limits for the distribution of ITS values.

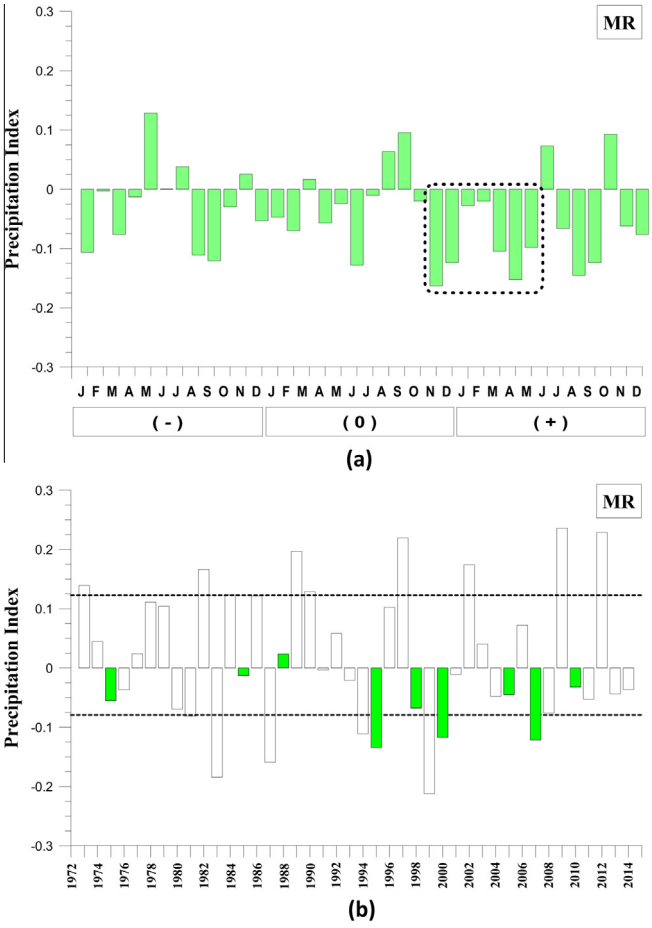

Fig. 11. As in Fig. 10, except for the candidate MR region.

into modular coefficients, the relationship between the La Niña composite cycle and the annual precipitation cycle plotted in Fig. 13. There exists a group of persistent below normal precipitation for the La Niña signal season in the La Niña–annual precipitation cycle, thus it is reasonable that the La Niña forcing modulates precipitation by decreasing its magnitude in the UR and MR region, respectively. According to the above results of the annual cycle analyses, El Niño forcing modulates precipitation by enhancing, while La Niña forcing modulates precipitation by suppressing for the signal seasons.

Based on the statistical hypothesis test by the Mann–Whitney *U* approach, the quantitative and noticeable difference between the two datasets of the warm and cold episodes was identified with the rate of significant relationship up to 74%. According to the above results, at the 0.10 significance level, there is enough evidence to suggest that average value of signal season associated with the warm episodes is different from (larger than) those in association with the cold episodes.

The results of calculating cross-correlation coefficients to examine the intensity and the trend (positive or negative) of the ENSO–Precipitation correlation are outlined in Table 6 and Fig. 14, on the basis of seasonal comparison between the large-scale climate index (categorized SOI) and the seasonal precipitation data (non-exceedance probability). As a general result, both analyses for two extreme phases of SO show significant correlations with the non-exceedance probability time series for the 0.05 significance level. The strongest positive correlation coefficients with the lag-4 seasons are calculated at all core regions, except the La Niña–UR region, under the Strong El Niño SOI condition. On the other hand, the strongest negative correlation coefficients with the same lag-4 seasons are found at all core regions under the Strong La Niña condition (see the underlined values in Table 6). As a result, the stronger intensity of the El Niño/La Niña forcing, the larger and smaller precipitation at overall South Korea with lag time 4 seasons.

Table 4
Probabilistic assessments for significance level based on the hypergeometric distribution (El Niño events).

Case	Region	*N*	*k*	*n*	*m*	Probability
A	UR	42	23	10	8	0.057
	MR	42	25	10	9	0.024
	LR	42	27	10	9	0.048
B	UR	42	9	9	3	0.209
	MR	42	9	9	4	0.067
	LR	42	9	9	4	0.067

Table 5
As in Table 4, except for La Niña events.

Case	Region	*N*	*k*	*n*	*m*	Probability
A	UR	42	20	9	7	0.040
	MR	42	23	9	8	0.021
B	UR	42	8	8	5	0.003
	MR	42	8	8	3	0.132

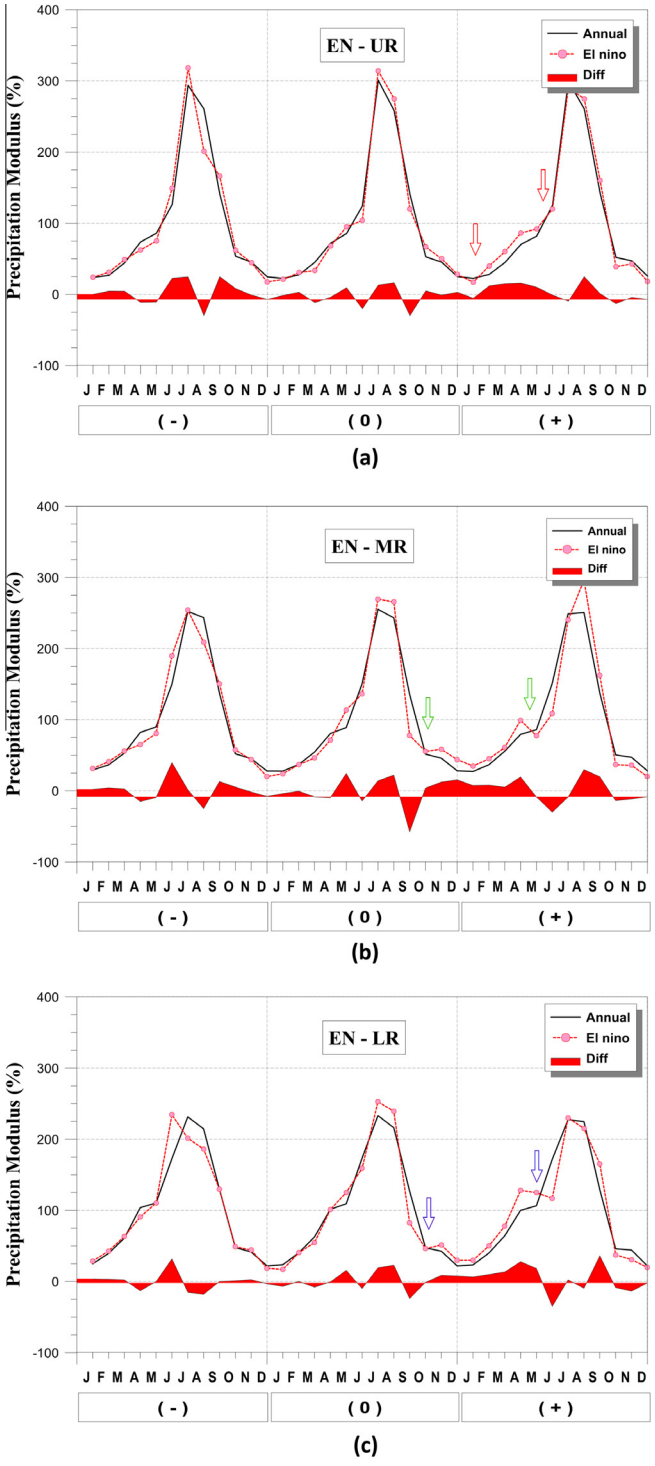

Fig. 12. The comparison of El Niño composite cycles (shown by dashed line) and annual cycles (shown by solid line) of (a) the UR, (b) MR, and (c) LR, based on modular coefficients. Arrows indicate the beginning and end months of the SO signal season.

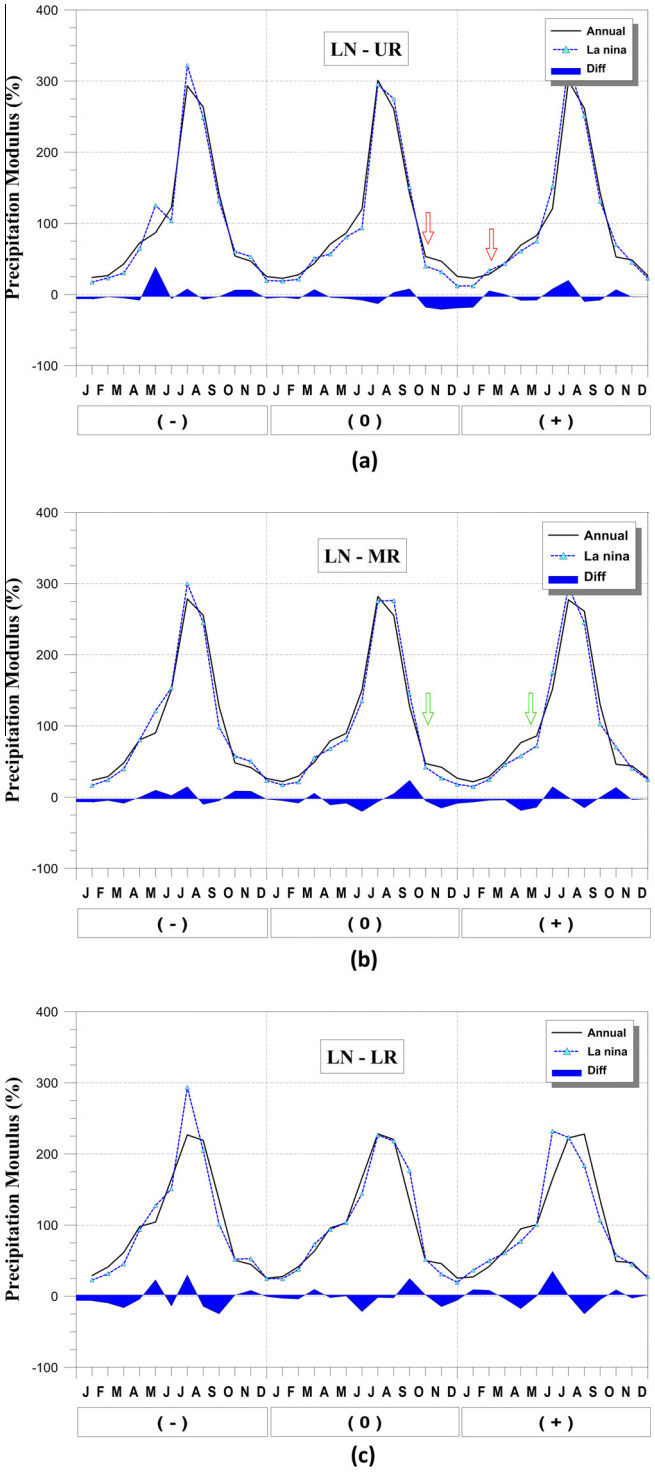

Fig. 13. As in Fig. 12, except for La Niña composite cycles.

3.4. Discussion

The results of the present analyses as shown in Figs. 6(a), 7(a), and 8(a), indicate a tendency for negative precipitation anomaly in early fall of the warm event year and positive precipitation departure for winter through spring of the following year over South Korea. Especially, the magnitude of the negative precipitation anomaly during September of the El Niño year is much larger than that of the same season of non-El Niño year. In contrast, the opposite tendency is observable during the cold events as shown in Figs. 10(a) and 11(a). The precipitation anomalies for the core regions are above normal for early fall of the La Niña year and below normal for winter through spring of the following year.

The physical teleconnection mechanisms behind the impacts of the ENSO forcing on the mid-latitude precipitation are not clear. Cha et al. (1999) investigated the relationship between the

Table 6
Cross-correlation coefficients with respect to regions.

Core region		Strong El Niño SOI				Normal condition				Strong La Niña SOI			
		Lag-1	Lag-2	Lag-3	Lag-4	Lag-1	Lag-2	Lag-3	Lag-4	Lag-1	Lag-2	Lag-3	Lag-4
El Niño	UR	−0.19	0.31	0.02	0.34	0.04	0.01	−0.02	0.15	0.07	0.21	−0.03	−0.26
	MR	0.03	0.08	0.16	0.61	0.00	0.06	−0.07	0.16	−0.04	0.15	−0.06	−0.29
	LR	0.07	0.27	−0.35	0.67	−0.01	0.10	0.03	0.11	−0.19	0.15	−0.05	−0.26
La Niña	UR	−0.06	0.32	−0.05	0.30	0.03	0.01	0.00	0.12	0.02	0.23	−0.10	−0.24
	LR	−0.33	0.32	0.33	0.52	0.01	0.04	−0.08	0.22	0.00	0.18	0.15	−0.38

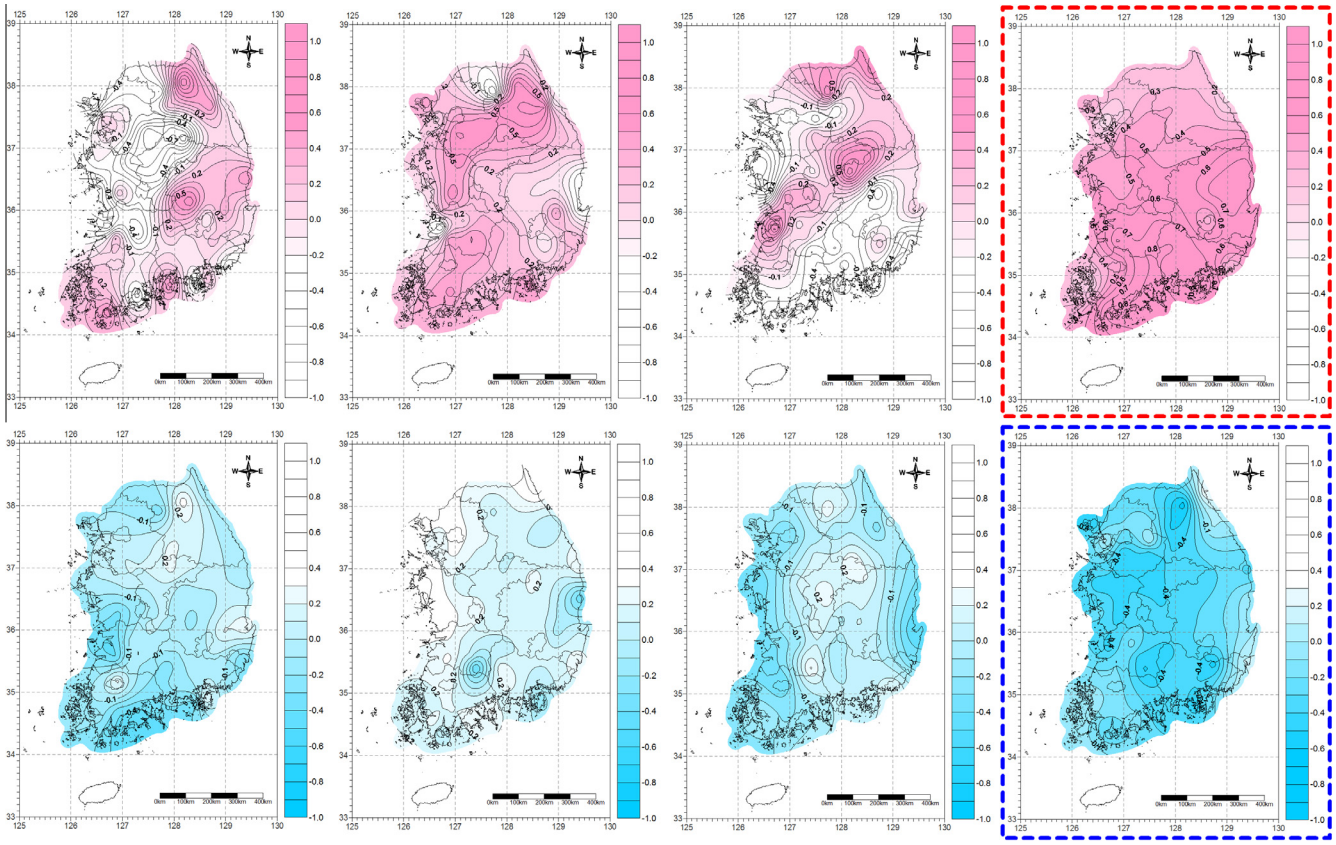

Fig. 14. Contour map of cross-correlation coefficients (CCC) between the seasonal precipitations and the categorized SOI series at different lags (from left to right, lag-1, lag-2, lag-3, lag-4) for Strong El Niño (upper) and Strong La Niña (lower).

extreme phases of ENSO cycles and the South Korean climate variations focusing on temperature, precipitation, cloud amount, etc., and indicated that ENSO forcing has a tendency to modulate the precipitation over Korea by enhancing or suppressing with respect to seasons. They pointed out that subtropical high shifts more southward than normal due to the inactive cumulus convection, which results in the weakening of its impact on Korea and Japan during the El Niño years. In contrast, during the La Niña years, subtropical high displaces northward compared with normal climatology due to the active convection, which causes the strengthening of its response to Korean and Japan. These features are conducive to the deficiency/sufficiency of early fall precipitation during El Niño/La Niña events over South Korea.

In addition to the position of subtropical high, it is plausible to explain the teleconnection based on the tropical cyclone activities affecting the overall Korean precipitation regime due to the fact that tropical cyclones generated over the western North Pacific play an important role in precipitation amount for the second rainy season in early fall over South Korea. In the western North Pacific, the monsoon trough associated with low-level cyclonic vorticity shifts eastward and reduces vertical wind shear during the warm phase of ENSO cycle (Chu, 2004). Li (1990) indicated that the western North Pacific tends to experience a decreased occurrence of tropical cyclones during El Niño years, and an increased occurrence of tropical cyclones during La Niña years. As a result, the suppressed precipitation in September is associated with the weakening of the second rainy season by decreased tropical cyclones during the evolution of the warm episode over East Asia, while the enhanced precipitation in September of the cold episode year is related to the strengthening of the second rainy season by increased tropical cyclones.

In a study of the Pacific–East Asia teleconnection (PEA), which is a mechanism that bonds sea surface temperature anomalies of central Pacific and climate variation in East Asia, Wang et al.

(2000) pointed out that systematic configuration of PEA teleconnection could be linked with the large-scale western North Pacific anomalous cyclone/anticyclone. The PEA teleconnection is confined to the lower troposphere and is a vorticity wave pattern arising from the central Pacific poleward and westward against the westerly jet stream. During the mature phases of ENSO, the western North Pacific wind anomalies progress and persist from late fall through subsequent winter and spring, causing enhanced/suppressed precipitation departures along the East Asian polar front by a weaker/stronger than normal winter monsoon. Consequently, the climate in South Korea is wetter/drier than normal during El Niño/La Niña winter and ensuing spring (Kang and Jeong, 1996). The results of the previous studies aforementioned are fairly in agreement with those of the present analysis.

In the global scale study associated with the ENSO–precipitation teleconnection by Ropelewski and Halpert (1987, 1989), conclusive findings of East Asia were not clearly described due to the scarcity of quantitative precipitation data. Based on a careful visual inspection of harmonic dial map of the above global scale study, several harmonic vectors are plotted without any consistent magnitude and phase angle because of the limitation of precipitation data. The stations for East Asia applied in the above study were insufficient to analysis the remote ENSO impact on the South Korean precipitation. This present study provides better insights and a substantial amount of information on the ENSO–precipitation teleconnections over a part of East Asian region that has not been documented by the previous studies.

Jin et al. (2005) identified significant correlations between the SOI and precipitation in Japan and Korea, using cross-correlation analysis using the categorized SOI classified by five groups according to their magnitudes. While they pointed out significant correlations (−0.61) between the strong La Niña SOI and precipitation in Busan located in southernmost part of the study area, the correlation coefficients from this present analysis are calculated as −0.24 to −0.38 under the strong La Niña SOI condition and 0.32 to 0.67 under the strong El Niño SOI condition on an average basis over the all core regions. The differences of the two analyses are attributed to the date scale and areal coverages for station (1:60), and the present study concurs with and extends the previous study.

In comparison with several recent studies concerning the ENSO–precipitation relationship over South Korea, the overall results are in good agreement with the findings of Cha et al. (1999) with respect to positive/negative signals during El Niño/La Niña events. Also, the September (0) driest/wettest condition for all core regions based on the aggregate composites of this analysis, coincides with the results of Shin (2002) in terms of the deficiency/sufficiency of early fall precipitation in El Niño/La Niña years.

Consequently, the overall findings of this diagnostic investigation are believed to provide additional confirmation to the climatic relationship between ENSO forcing and hydrometeorological variability over mid-latitude area.

4. Summary and conclusion

In this investigation, the remote impacts of the extreme phases of the Southern Oscillation (SO), i.e., the El Niño and La Niña events, on the monthly precipitation patterns over South Korea are examined based on the composite and harmonic analysis. The overall results of the ENSO–precipitation teleconnections are summarized as follows with the details of the analysis outlined in Tables 2 and 3. According to the composite and harmonic analysis, the three core regions, namely the Upper Region (UR), the Middle Region (MR), and the Lower Region (LR), were determined with a high level of the spatial coherence and temporal consistency rate which represent the geographical extent and magnitude of the response of the ENSO forcing to the precipitation patterns.

The main conclusions of this investigation are:

(1) El Niño–precipitation relationships; the precipitation anomalies are below normal for early fall of the event year and above normal for winter through spring of the following year. For UR, the February (+) to May (+) wet period is the season having a high level of coherence and consistency. For MR and LR, the November (0) to April (+) and November (0) to May (+) wet periods are the signal season showing a strong and consistent teleconnection. The spatial coherence rates of UR, MR, and LR for El Niño events are 0.94, 0.98, and 0.98 and the temporal consistency rates of each region for the warm episodes are 0.80, 0.90, and 0.80.

(2) La Niña–precipitation relationships; the precipitation anomalies are above normal for early fall of the event year and below normal for winter through spring of the following year. According to the harmonic analysis, the apparent signal season for the dry period are October (0)–January (+) for UR and November (0)–May (+) for MR. The spatial coherence rates of UR, MR, and LR are 0.98, 0.96, and 0.94 and the temporal consistency rates of UR and MR for the cold episodes are both 0.78, while there is no apparent evident season to be accepted as core region with a climatic signal in LR.

(3) A comparative analysis between El Niño and La Niña–precipitation relationships reveals high statistical significance levels for the above/below normal precipitation with the reversal of the sign for both ENSO cycles, i.e., positive and negative responses respectively. Furthermore, the wet anomalies during the warm event years are more remarkable and significant than the dry departures during the cold event years due to the fact that three core regions are detected for El Niño–precipitation relationships while two core regions are identified for La Niña–precipitation relationships. Based on the annual cycle analysis, El Niño forcing modulates precipitation by enhancing, while La Niña forcing modulates precipitation by suppressing for the signal seasons. Moreover, Mann–Whitney *U* hypothesis test implies that the average value of signal season associated with the warm episodes is larger than those in association with the cold episodes. Additionally, the overall outcomes of cross-correlation analysis between the seasonal precipitation and the categorized SOI confirm the implied teleconnections between the tropical Southern Oscillation phenomenon and precipitation over South Korea, with positive and negative correlation with a lag time of 4 seasons.

In conclusion, the climatic teleconnections between the extreme phase of SO and mid-latitude precipitation are identified over South Korea.

References

Berlage, H.P., 1966. The Southern Oscillation and world weather. Meteor. Inst. Meded. Verh. 88, 152.

Bradley, R.S., Diaz, H.F., Kiladis, G.N., Eischeid, J.K., 1987. ENSO signal in continental temperature and precipitation records. Nature 327, 487–501.

Brooks, C.E.P., Carruthers, N., 1953. Handbook of Statistical Methods in Meteorology. Her Majesty's Stationery Office, London.

Cai, W., Rensch, P.V., Cowan, T., 2011. Teleconnection pathways of ENSO and the IOD and the mechanisms for impacts on Australian rainfall. J. Clim. 24, 3910–3923.

Cha, E.J., Jhun, J.G., Chung, H.S., 1999. A study on characteristics of climate in South Korea for El Niño/La Niña years. J. KMS 35 (1), 99–117 (in Korean).

Chandimala, J., Zubair, L., 2007. Predictability of streamflow and rainfall based on ENSO for water resources management in Sri Lanka. J. Hydrol. 335, 303–312.

Chu, P.S., 2004. ENSO and tropical cyclone activity. In: Columbia University Press, pp. 297–332.
Dai, A., 2013. The influence of the inter-decadal Pacific oscillation on US precipitation during 1923–2010. Clim. Dyn. 41, 633–646.
Douglas, A.E., Englehart, P.J., 1981. On a statistical relationship between autumn rainfall in the central equatorial pacific and subsequent winter precipitation in Florida. Mon. Weather Rev. 109, 2377–2382.
Guttman, N.B., 1998. Comparing the Palmer drought index and the standardized precipitation index. J. Am. Water Resour. Assoc. 34 (1), 113–121.
Haan, C.T., 1977. Statistical Methods in Hydrology. Iowa State University Press, Ames, IA.
Halpert, M.S., Ropelewski, C.F., 1992. Surface temperature patterns associated with the Southern Oscillation. J. Clim. 5, 557–593.
Horn, L.H., Bryson, R.A., 1960. Harmonic analysis of the annual march of precipitation over the United States. Ann. Assoc. Am. Geor. 50, 157–171.
Hsu, C.F., Wallace, J.M., 1976. The global distribution of the annual and semiannual cycles in precipitation. Mon. Weather Rev. 104, 1093–1101.
Jin, Y.H., Kawamura, A., Jinno, K., Berndtsson, R., 2005. Quantitative relationship between SOI and observed precipitation in southern Korea and Japan by nonparametric approaches. J. Hydrol. 301, 54–65.
Kahya, E., Dracup, J.A., 1993. US streamflow patterns in relation to the El Niño/Southern Oscillation. Water Resour. Res. 29 (8), 2491–2503.
Kahya, E., Dracup, J.A., 1994. The influences of type 1 El Niño and La Niña events on streamflows in the Pacific southwest of the United States. J. Clim. 7, 965–976.
Kang, I., Jeong, Y., 1996. Association of interannual variations of temperature and precipitation in Seoul with principal modes of Pacific SST. J. Korean Meteor. Soc. 32, 339–345.
Karabörk, M.Ç., Kahya, E., 2003. The teleconnections between extreme phases of Southern Oscillation and precipitation patterns over Turkey. Int. J. Climatol. 23, 1607–1625.
Kiladis, G.N., Diaz, H.F., 1989. Global climatic anomalies associated with extremes in the Southern Oscillation. J. Clim. 2, 1069–1090.
King, A.D., Klingaman, N.P., Alexander, L.V., Donat, M.G., Jourdain, N.C., Maher, P., 2014. Extreme rainfall variability in Australia: patterns, drivers, and predictability. J. Clim. 27, 6035–6050.
Klingaman, N.P., Woolnough, S.J., Syktus, J., 2013. On the drivers of inter-annual and decadal rainfall variability in Queensland, Australia. Int. J. Climatol. 33, 2413–2430.
Lee, D.R., 1998. Relationships of El Niño and La Niña with both temperature and precipitation in South Korea. J. KWRA 31 (6), 807–819 (in Korean).
Li, C., 1990. On the interaction between anomalous circulation/climate in East Asia and El Niño event. Clim. Change Dyn. Model., 101–126 (TISC August 12–20)
McBride, J.L., Nicholls, N., 1983. Seasonal relationships between Australian rainfall and the Southern Oscillation. Mon. Weather Rev. 111, 1998–2004.
McKee, T.B., Doesken, N.J., Kleist, J., 1993. The relationship of drought frequency and duration to time series. In: 8th Conference on Applied Climatology, Anaheim, CA, 1993, pp. 179–187.
Power, S.B., Haylock, M., Colman, R., Wang, X., 2006. The predictability of interdecadal changes in ENSO activity and ENSO teleconnection. J. Clim. 19, 4755–4771.
Price, C., Stone, L., Huppert, A., Rajagopalan, B., Alpert, P., 1998. A possible link between El Niño and precipitation in Israel. Geophys. Res. Lett. 25, 3963–3966.
Quinn, W.H., Zopf, D.O., Short, K.S., Kuo Yang, R.T.W., 1978. Historical trends and statistics of the Southern Oscillation, El Niño, and Indonesian droughts. Fish. Bull. 76, 663–678.
Rasmusson, E.M., Carpenter, T.H., 1983. The relationship between eastern equatorial Pacific sea surface temperatures and rainfall over India and Sri Lanka. Mon. Weather Rev. 111, 517–528.
Rasmusson, E.M., Wallace, J.M., 1983. Meteorological aspects of the El Niño/southern oscillation. Science 222, 1195–1202.
Redmond, K.T., Koch, R.W., 1991. Surface climate and streamflow variability in the western United States and their relationship to large circulation indices. Water Resour. Res. 27 (9), 2381–2399.
Ropelewski, C.F., Halpert, M.S., 1986. North American precipitation and temperature patterns associated with El-Niño-Southern oscillation (ENSO). Mon. Weather Rev. 114, 2165–2352.
Ropelewski, C.F., Halpert, M.S., 1987. Global and regional scale precipitation patterns associated with the El Niño/Southern Oscillation. Mon. Weather Rev. 115, 1606–1626.
Ropelewski, C.F., Halpert, M.S., 1989. Precipitation patterns associated with the high index phase of the southern oscillation. J. Clim. 2, 268–284.
Scott, C.M., Shulman, M.D., 1979. An areal temporal analysis of precipitation in the Northeastern United States. J. Appl. Meteorol. 18, 627–633.
Shin, H.S., 2002. Do El Niño and La Niña have influences on South Korean hydrologic properties? In: Proceedings of the 2002 Annual Conference, Japan Society of Hydrology and Water Resources, pp. 276–282.
Shukla, J., Paolino, D.A., 1983. The southern oscillation and long-range forecasting of summer monsoon rainfall over India. Mon. Weather Rev. 111, 1830–1837.
Trenberth, K.E., 1997. The definition of El Niño. Bull. Am. Meteorol. Soc. 78, 2771–2777.
Walker, G.T., 1923. Correlation in seasonal variations of weather: VIII. A preliminary study of world weather. Mem. Indian Meteorol. Dept. 24, 75–131.
Walker, G.T., Bliss, E.W., 1932. World weather V. Mem. Roy. Meteor. Soc. 4 (36), 53–84.
Wang, B., Wu, R., Fu, X., 2000. Pacific–East Asian teleconnection: how does ENSO affect East Asian climate. J. Clim. 13, 1517–1536.
Westra, S., Alexander, L.V., Zwiers, F.W., 2013. Global increasing trends in annual maximum daily precipitation. J. Clim. 26, 3904–3918.
Wilks, D.S., 1995. Statistical Methods in Atmospheric Sciences. Academic Press, 330–334.
WMO, 2014. El Niño/Southern Oscillation. WMO-No. 1145, 2–4.